

USING HYDRODYNAMICAL SIMULATIONS OF STELLAR ATMOSPHERES FOR PERIODOGRAM STANDARDIZATION : APPLICATION TO EXOPLANET DETECTION

S. Sulis, D. Mary, L. Bigot

Laboratoire Lagrange, UMR CNRS 7293, Université Côte d'Azur,
Observatoire de la Côte d'Azur, CS 34229, 06304 Nice, France

ABSTRACT

Our aim is to devise a detection method for exoplanet signatures (multiple sinusoids) that is both powerful and robust to partially unknown statistics under the null hypothesis. In the considered application, the noise is mostly created by the stellar atmosphere, with statistics depending on the complicated interplay of several parameters. Recent progresses in hydrodynamic (HD) simulations show however that realistic stellar noise realizations can be numerically produced off-line by astrophysicists. We propose a detection method that is calibrated by HD simulations and analyze its performances. A comparison of the theoretical results with simulations on synthetic and real data shows that the proposed method is powerful and robust.

Index Terms— Detection, periodogram, colored noise, standardization, statistics.

1. INTRODUCTION

This study is motivated by the long-standing challenge of detecting rocky low mass exoplanets. In this aim, future instruments with extremely low detector noise are being developed, giving access to massive time series of observations (high sampling rates of typically five samples per minute, for several months to years, see e.g. [1, 2, 3]). We focus on the so-called radial velocity data, where the planet signature (if present) appears as one or a few sinusoidal components of weak amplitudes w.r.t. the noise level [4]. For the considered new observing facilities, the main noise source will not come from the instrument but from the stochastic activity of the star itself (convection, magnetic dynamo, stellar spots and oscillations).

Sinusoid detection is another long-standing problem. In various fields, including indeed Statistics and Astronomy, a particularly rich amount of methods exists, a central piece of which is the (Schuster's) periodogram [5] :

$$P(\nu) := \frac{1}{N} \left| \sum_{j=1}^N X(t_j) e^{-i2\pi\nu t_j} \right|^2. \quad (1)$$

In Eq.(1), $X(t)$ will be an evenly sampled time series obtained at N epochs t_j , with sampling rate $\Delta t = t_{j+1} - t_j, \forall j \in \{1, \dots, N-1\}$. The type I errors (or false alarms, FA) of any test based on the ordinates of P depend on the statistics of these ordinates under the null hypothesis. In practice, the statistics of the noise are often not (or only partially) known, and so are those of the P ordinates. In this case, it is difficult to assess how reliable is any claimed detection.

In Statistical signal processing, some classical tests (e.g. [6, 7, 8]) partially cope with this issue by guaranteeing the control of the FA rate whatever the unknown noise variance, provided that the noise is Gaussian, independent and identically distributed (i.i.d.). When the noise is not white but colored in some unknown manner, a classical approach consists in calibrating $P(\nu)$ by some estimate $\hat{P}(\nu)$, leading to a frequency-wise standardized periodogram of the form $\frac{P(\nu)}{\hat{P}(\nu)}$. Usually, the noise Power Spectral Density (PSD)

has to be estimated from the data. This can be done through non-parametric methods (e.g. local SNR [9], modified periodogram smoothers [10, 11], robust M-estimators [12, 13]) or parametric methods (e.g. iterative Yule-Walker [14], ratio of autoregressive (AR) spectral estimates [15], balanced model truncation [16]). Even if some of these estimators are asymptotically unbiased, the unavoidable injection of estimation noise in the denominator of the standardized periodogram makes the statistical characterization of the test statistics difficult. One can resort to Monte Carlo or bootstrap simulations [17] to evaluate the thresholds empirically (see [18], Chap.7 for examples of gaps between theoretical and empirical thresholds), but this procedure may not be tractable for massive time series (large N).

In Astronomy, preprocessing stages aimed at “whitening” the noise (e.g. with local trend filtering or line removal with the CLEAN method [19]) or based on various ARMA (AR-Moving Average) noise models [20] are most often applied to the data before conducting the detection test. Such procedures pose the same question of robustness about the actual FA rate at which the test is conducted. In presence of unknown colored noise, the reliability of a claimed detection of a low mass telluric planet is thus difficult to assess (see for instance the recent and controversial case of α Centauri B [21, 22]).

In the present work, we do not attempt to build dedicated parametric noise models. We choose instead to exploit recent progresses in HD simulations [23]. These results demonstrate that reliable time series of the stellar noise can be simulated by numerical codes, which account for the complex interplay of various astrophysical processes in the star's interior. We assume that a training data set (in the form of time series) is available and use this information to standardize the periodogram. The data set is considered unbiased, but possibly limited in size, because HD simulations are heavy. In fact, simulating 100 days at high sampling rate requires around 3 calculation months over 120 CPU. Consequently, realistic numbers of simulated light curves available in practice will not be more than, say, a hundred. This raises the question of the impact of estimation noise in the proposed standardization approach.

Addressing this question first requires, for the two hypotheses of our model (Sec.2), the investigation of the statistics of the classical, averaged and standardized periodograms. This is the purpose of Sec.3, where the use of asymptotic results is motivated by the large duration and high sampling rate (large N) considered here. The second step is to select several tests (Sec.4) for which the benefits gained from the proposed standardization can be highlighted and quantified. We opt for a sample of classical tests covering the different cases of single and multiple sinusoids detection. At this stage we are in position to derive the tests statistics and the corresponding FA (Sec.5) and detection (Sec.6) rates. The last step is a numerical evaluation of the theoretical results, the method performances and its actual robustness (Sec.7).

2. STATISTICAL MODEL

We consider two hypotheses :

$$\begin{cases} \mathcal{H}_0 : X(t_j) = \epsilon(t_j) \\ \mathcal{H}_1 : X(t_j) = \sum_{i=1}^{N_s} \alpha_i \sin(2\pi f_i t_j + \phi_i) + \epsilon(t_j) \end{cases} \quad (2)$$

where $X(t_j = j\Delta t)$ is the evenly sampled data time series and $\epsilon(t_j)$ a zero-mean second-order stationary Gaussian noise with PSD $S_\epsilon(\nu)$ and autocorrelation function r_ϵ , for which $\inf(S_\epsilon(\nu)) > 0$ and $\sum_k |r_\epsilon(k)| < \infty$. The N_s amplitudes α_i , frequencies f_i and phases ϕ_i represent the planet signatures and are unknown.

3. PERIODOGRAMS' STATISTICS : ASYMPTOTICS

3.1. Classical (Schuster's) periodogram

Without loss of generality and to simplify the presentation, N is even and the considered frequencies in Eq.(1) belong to the subset of $\frac{N}{2} - 1$ Fourier frequencies $\nu_k = \{\frac{k}{T}\}$ where $k \in \Omega := \{1, \dots, \frac{N}{2} - 1\}$. Asymptotically, the periodogram P is an unbiased but inconsistent estimate of the PSD [24]. However, under the above assumptions on ϵ , the periodogram ordinates at different frequencies ν_k and $\nu_{k'}$ are asymptotically independent [18].

Under \mathcal{H}_0 , the asymptotic distribution of P is ([24], theorem 5.2.6) :

$$P(\nu_k|\mathcal{H}_0) \sim \frac{S_\epsilon(\nu_k)}{2} \chi_2^2, \quad \forall k \in \Omega. \quad (3)$$

The χ_2^2 is a χ_1^2 at $k = 0, \frac{N}{2}$. We restrict to Ω for simplicity. Under \mathcal{H}_1 , the distribution of $P(\nu_k)$ can be found in the complex case in [18], Corollary 6.2. Using this corollary and Euler's formula for the sines in model (2), we obtain that, for large N , $P(\nu_k)$ is approximately distributed as :

$$P(\nu_k|\mathcal{H}_1) \sim \frac{S_\epsilon(\nu_k)}{2} \chi_{2, \lambda_k}^2, \quad \forall k \in \Omega, \quad (4)$$

with $\lambda_k = \lambda(\nu_k)$ a non-centrality parameter expressing the spectral leakage of all signal frequencies at location ν_k . Generally, this leakage is caused by the fact that the $\{f_i\}$ do not belong to the natural Fourier grid defined by Ω . Denoting by $K_N(\nu) = \left(\frac{\sin(N\pi\nu)}{N\sin(\pi\nu)}\right)^2$ the Fejér kernel (or spectral window), the asymptotic expression of the parameters λ_k , $k \in \Omega$ for model (2) writes :

$$\begin{aligned} \lambda(\nu_k) = & \frac{N}{2S_\epsilon(\nu_k)} \sum_{i=1}^{N_s} \alpha_i^2 \left[K_N(f_i - \nu_k) + K_N(f_i + \nu_k) \right. \\ & \left. + 2 \frac{\sin(N\pi(f_i - \nu_k))}{N\sin(\pi(f_i - \nu_k))} \frac{\sin(N\pi(f_i + \nu_k))}{N\sin(\pi(f_i + \nu_k))} \cos(2\pi(N+1)f_i + 2\phi_i) \right]. \end{aligned} \quad (5)$$

3.2. Averaged periodogram

We assume that a training data set \mathcal{T} of independent realizations of the stellar noise is available. This set is obtained by HD simulations and composed with L times series X_ℓ sampled on the same grid as the observations : $\mathcal{T} = \{X_\ell(t_j), j = 1, \dots, N, \ell = 1, \dots, L\}$. A straightforward, consistent and unbiased estimate of the noise PSD can be obtained by the averaged periodogram [25] :

$$\bar{P}(\nu|\mathcal{H}_0) := \frac{1}{L} \sum_{\ell=1}^L \frac{1}{N} \left| \sum_{j=1}^N X_\ell(t_j) e^{-i2\pi\nu t_j} \right|^2,$$

whose asymptotic distribution can be easily obtained using (3) as :

$$\bar{P}(\nu_k|\mathcal{H}_0) \sim \frac{S_\epsilon(\nu_k)}{2L} \chi_{2L}^2, \quad \forall k \in \Omega. \quad (6)$$

Note that in this setting, any source of bias (caused for instance by imperfect HD simulations) is left out of scope of this study. The focus is on the stochastic estimation noise caused by the finiteness of \mathcal{T} , which is encapsulated in L and impacts the distribution of \bar{P} .

3.3. Standardized periodogram

The standardized periodogram considered here is defined as :

$$\tilde{P}(\nu_k) := \frac{P(\nu_k)}{\bar{P}(\nu_k)}. \quad (7)$$

As the numerator and denominator are independent variables with known asymptotic distributions, assessing the distribution of their ratio is straightforward. The ratio of two independent random variables (r.v.) $V_1 \sim \chi_{d_1}^2$ and $V_2 \sim \chi_{d_2}^2$ follows a Fisher-Snedecor law noted $F(d_1, d_2)$ with (d_1, d_2) degrees of freedom : $\frac{V_1/d_1}{V_2/d_2} \sim F(d_1, d_2)$ [26]. Consequently, from (3) and (6), the asymptotic distribution of \tilde{P} under \mathcal{H}_0 is :

$$\tilde{P}(\nu_k|\mathcal{H}_0) \sim \frac{S_\epsilon(\nu_k)\chi_2^2/2}{S_\epsilon(\nu_k)\chi_{2L}^2/2L} \sim F(2, 2L), \quad \forall k \in \Omega. \quad (8)$$

Similarly, under \mathcal{H}_1 , we deduce the asymptotic distribution of \tilde{P} with (4) and (6) :

$$\tilde{P}(\nu_k|\mathcal{H}_1) \sim \frac{\chi_{2, \lambda_k}^2/2}{\chi_{2L}^2/2L} \sim F_{\lambda_k}(2, 2L), \quad \forall k \in \Omega, \quad (9)$$

with λ_k given by (5). These results call for two remarks. First, an F distribution similar to that of (8) was obtained in [27] when using ratios of the form $P(\nu_k)/P(\nu_l)$, $k \neq l$ (for symmetry testing purposes). Second, (8) shows that the distribution of the standardized periodogram is independent of the (partially unknown) noise PSD, which is indeed a necessary condition for a robust detection test.

4. STATISTICAL TESTS

The first three tests below are considered for comparison purposes. The three other tests are the counterpart of classical tests applied to \tilde{P} instead of P (many more such tests could be devised). In the following, the order statistics of the periodograms will be noted with parentheses. For instance, the order statistics of P are : $\min_k P(\nu_k) = P_{(1)} < P_{(2)} < \dots < P_{(\frac{N}{2}-1)} = \max_k P(\nu_k)$.

4.1. Classical tests

Perhaps the most classical reference test (including in Astronomy) is the Fisher test :

$$T_{Fi} \underset{\mathcal{H}_0}{\overset{\mathcal{H}_1}{\geq}} \gamma, \quad \text{with} \quad T_{Fi} := \frac{P_{(\frac{N}{2}-1)}}{\sum_{k \in \Omega} P_{(k)}}, \quad (10)$$

where $\gamma \in \mathbb{R}^+$ is a threshold that determines the FA rate. This test is robust to an unknown noise variance [28], but the noise must be white Gaussian. When this is the case, the denominator of (10) is an asymptotically unbiased estimate of the PSD (to a constant) [11]. Under \mathcal{H}_1 , for a model involving a single sinusoid f_1 on the Fourier grid, the Generalized Likelihood Ratio (GLR) test corresponds to $P_{(N/2-1)} \underset{\mathcal{H}_0}{\overset{\mathcal{H}_1}{\geq}} \gamma$ [29]. So, under \mathcal{H}_0 , the Fisher test can be seen as a standardization of the GLR by the estimated variance $\hat{\sigma}^2 \propto \sum_{k \in \Omega} P(\nu_k)$.

In the case of multiple sinusoids ($N_s > 1$), the performances of the Fisher test are known to decrease, owing to the perturbations of sinusoids in the noise variance estimation. Many alternatives exist, e.g. [30, 11]. These tests attempt to better estimate the noise level by

excluding a number N_c of ordinates presumably contaminated by the sinusoids (see [11, 18, 24]). Two such tests, offering the same robustness against unknown variance, are the robust Fisher test [18] and the Chiu test [7] defined by $T_{Fi,rob} \gtrsim_{\mathcal{H}_0}^{\mathcal{H}_1} \gamma$ and $T_{Ch} \gtrsim_{\mathcal{H}_0}^{\mathcal{H}_1} \gamma$, where :

$$T_{Fi,rob} := b_r \left(\frac{N}{2} - 1 \right) r \frac{P_{(\frac{N}{2}-1)}}{\sum_{k=1}^{\frac{N}{2}-1-N_c} P_{(k)}}, \quad T_{Ch} := \frac{P_{(\frac{N}{2}-N_c)}}{\sum_{k=1}^{\frac{N}{2}-1-N_c} P_{(k)}}, \quad (11)$$

with $r = \frac{\frac{N}{2}-1-N_c}{\frac{N}{2}-1}$ and $b_r = 1 + r^{-1}(1-r) \log(1-r)$. Note that the last two approaches pose the question of the choice of N_c . Not fixing N_c in advance but estimating this parameter from the data may lead to a more powerful test, but at the cost of a weaker control of the FA rate (as N_c is random). To avoid this complication, the tests will be compared in the numerical study for N_c set to N_s .

4.2. Tests based on the standardized periodogram

Under \mathcal{H}_0 and in the asymptotic regime, \tilde{P} in (7) is i.i.d. since the ratio cancels out the frequency dependence on the PSD.

If $N_s = 1$, the following simple test is thus likely to be powerful :

$$\tilde{T} \gtrsim_{\mathcal{H}_0}^{\mathcal{H}_1} \gamma, \quad \text{with} \quad \tilde{T} := \tilde{P}_{(\frac{N}{2}-1)}. \quad (12)$$

Similarly, the discussion above suggests to consider Fisher's approach and to apply test (10) to (7) :

$$\tilde{T}_{Fi} \gtrsim_{\mathcal{H}_0}^{\mathcal{H}_1} \gamma, \quad \text{with} \quad \tilde{T}_{Fi} := \frac{\tilde{P}_{(\frac{N}{2}-1)}}{\sum_{k \in \Omega} \tilde{P}_{(k)}}. \quad (13)$$

Finally, in the case of several sinusoids, the good results of Chiu's test suggest to look for deviations in the region of the N_c^{th} largest \tilde{P} ordinate, $\tilde{P}_{(\frac{N}{2}-N_c)}$, instead of the largest one, $\tilde{P}_{(\frac{N}{2}-1)}$:

$$\tilde{T}_{Nc} \gtrsim_{\mathcal{H}_0}^{\mathcal{H}_1} \gamma, \quad \text{with} \quad \tilde{T}_{Nc} := \tilde{P}_{(\frac{N}{2}-N_c)}. \quad (14)$$

5. STATISTICS UNDER \mathcal{H}_0 AND FALSE ALARM RATE

The accurate control of the false alarm probability (P_{FA}) in case of partially unknown colored noise is a critical point. We now show that while this control is (not surprisingly) problematic with classical tests like (10, 11), the proposed tests (12, 14) allow such a control. We investigate first the tests T_{Fi} , \tilde{T}_{Fi} and \tilde{T} (designed for single sinusoid detection). Under \mathcal{H}_0 , their test statistics involve the largest value of a set of $\frac{N}{2} - 1$ r.v., $T_{Fi}(n)$, $\tilde{T}_{Fi}(n)$ and $\tilde{T}(n)$, whose definitions and distributions are given by, using (4) and (8) :

$$\begin{aligned} T_{Fi}(n) &:= \frac{P(\nu_n)}{\sum_{k \in \Omega} P(\nu_k)} \underset{as, ni, ni.d.}{\sim} \frac{\chi_2^2 S_\epsilon(n)/2}{\sum_{k \in \Omega} \chi_2^2 S_\epsilon(k)/2}, \\ \tilde{T}_{Fi}(n) &:= \frac{\tilde{P}(\nu_n)}{\sum_{k \in \Omega} \tilde{P}(\nu_k)} \underset{as, ni, i.d.}{\sim} \frac{F(2, 2L)}{\sum_{k \in \Omega} F(2, 2L)}, \\ \tilde{T}(n) &:= \tilde{P}(n) \underset{as, ni, i.d.}{\sim} F(2, 2L), \end{aligned} \quad (15)$$

where “as, ni, ni.d.” means asymptotically non independent and non identically distributed. In the first case, each r.v. $T_{Fi}(n)$ clearly depends on the unknown PSD. In the second case, each r.v. $\tilde{T}_{Fi}(n)$ is a ratio of a F variable over a sum of F variables. To our knowledge, there is no analytic characterization of the resulting distribution. Hence, in both cases, assessing the distribution of the maximum of these variables is problematic. In the third case, the $\tilde{T}(n)$

r.v. are independent and follow a F distribution with known density φ_F [26]. Using the incomplete Beta function $B(d_1, d_2)$ and noting that $B(1, L) = \int_0^1 (1-t)^{L-1} dt = \frac{1}{L}$ we obtain :

$$\varphi_F(\gamma, 2, 2L) = \frac{1}{B(1, L)} \cdot \frac{1}{L} \cdot \left(1 + \frac{\gamma}{L}\right)^{-L-1} = \left(1 + \frac{\gamma}{L}\right)^{-L-1}.$$

It can be checked that the norm of $\varphi_F(\gamma, 2, 2L)$ is 1. Turning to the CDF $\Phi_F(\gamma, 2, 2L)$ of $\tilde{T}(n)$, we obtain by using $F(\gamma, d_1, d_2) = I_{\frac{d_1 \gamma}{d_1 \gamma + d_2}}(\frac{d_1}{2}, \frac{d_2}{2})$ [26] or by direct integration of $\varphi_F(\gamma, 2, 2L)$:

$$\Phi_F(\gamma, 2, 2L) = 1 - \left(\frac{L}{\gamma + L}\right)^L. \quad (16)$$

The P_{FA} can be computed thanks to the asymptotic independence of the $\{\tilde{T}(n)\}$:

$$\begin{aligned} P_{FA}(\tilde{T}, \gamma) &:= \Pr(\max_n \tilde{T}(n) > \gamma | \mathcal{H}_0) = 1 - \prod_n \Pr(\tilde{T}(n) \leq \gamma | \mathcal{H}_0) \\ &= 1 - \left(\Phi_F(\gamma, 2, 2L)\right)^{\frac{N}{2}-1} = 1 - \left(1 - \left(\frac{L}{\gamma + L}\right)^L\right)^{\frac{N}{2}-1}, \end{aligned} \quad (17)$$

which is a remarkably simple expression.

We turn now to the tests $T_{Fi,rob}$, T_{Ch} and \tilde{T}_{Nc} (designed for multiple sinusoids detection). The asymptotic distributions of the first two tests are known under the WGN assumption [7]. Using the same reasoning as above for T_{Fi} , it is easy to see that the noise PSD affects the distribution of the order statistics involved in these tests, with uncontrollable impact on the P_{FA} . Turning to \tilde{T}_{Nc} , remark that the number K of ordinates \tilde{P} larger than γ follows a binomial distribution : $K \sim \mathcal{B}(\frac{N}{2} - 1, 1 - \Phi_F(\gamma, 2, 2L))$, from which, with (16), we obtain :

$$\begin{aligned} P_{FA}(\tilde{T}_{Nc}, \gamma) &:= \Pr(\tilde{T}_{Nc} > \gamma | \mathcal{H}_0) = 1 - \sum_{i=0}^{N_c-1} \Pr(K = i) \\ &= 1 - \sum_{i=0}^{N_c-1} \binom{N/2-1}{i} \left(\frac{L}{\gamma + L}\right)^{Li} \left(1 - \left(\frac{L}{\gamma + L}\right)^L\right)^{\frac{N}{2}-1-i}. \end{aligned} \quad (18)$$

6. STATISTICS UNDER \mathcal{H}_1 AND DETECTION RATE

Under \mathcal{H}_1 , the same approach shows that one can not control the distribution of the r.v. $T_{Fi}(n)$ and $\tilde{T}_{Fi}(n)$ and consequently the associated detection probabilities (P_{DET}). In contrast, from (9) and using the same reasoning as for the P_{FA} , the P_{DET} of \tilde{T} is :

$$P_{DET}(\tilde{T}, \gamma) := \Pr(\max_n \tilde{T}(n) > \gamma | \mathcal{H}_1) = 1 - \prod_{k \in \Omega} \Phi_{F_{\lambda_k}}(\gamma, 2, 2L). \quad (19)$$

With (17) the relationship $\gamma(P_{FA})$ for \tilde{T} can be derived as :

$$\gamma(\tilde{T}, P_{FA}) = L \left[\left(1 - (1 - P_{FA})^{\frac{1}{\eta}}\right)^{-\frac{1}{L}} - 1 \right], \quad (20)$$

where $\eta = \frac{N}{2} - 1$. With (19) and (20), we deduce :

$$P_{DET}(\tilde{T}, P_{FA}) = 1 - \prod_{k \in \Omega} \Phi_{F_{\lambda_k}}(L[(1 - (1 - P_{FA})^{\frac{1}{\eta}})^{-\frac{1}{L}} - 1], 2, 2L), \quad (21)$$

which can be used to compute the ROC curves.

The function $\gamma \mapsto P_{DET}(\gamma)$ of the test \tilde{T}_{Nc} can be deduced similarly to (18), with the difference that K is no longer binomial owing to the λ_k . Denote by $\Omega^{(i)}$ one particular combination of i indices taken in Ω and $\bar{\Omega}^{(i)} := \Omega \setminus \Omega^{(i)}$ the set of remaining indices. Let $\{\Omega_1^{(i)}, \dots, \Omega_i^{(i)}\}$ (resp. $\{\bar{\Omega}_1^{(i)}, \dots, \bar{\Omega}_{\frac{N}{2}-1-i}^{(i)}\}$) denote the indices in

two such combinations, and let Ω^i (resp. $\bar{\Omega}^i$) be the set of all the $\{\Omega^{(i)}\}$ (resp. of all $\{\bar{\Omega}^{(i)}\}$). With these notations we obtain :

$$P_{\text{DET}}(\tilde{T}_{N_c}, \gamma) = 1 - \sum_{i=0}^{N_c-1} \sum_{\Omega^{(i)} k=1}^i \prod_{k=1}^i (1 - \Phi_{F_{\lambda_{\Omega_k^{(i)}}}(\gamma, 2, 2L)}) \prod_{k'=1}^{N-1-i} \Phi_{F_{\lambda_{\Omega_{k'}^{(i)}}}(\gamma, 2, 2L)}, \quad (22)$$

which is typographically heavy but can be used to compute ROC curves (in Eq.(22) the non-centrality parameters are given by (5)).

7. NUMERICAL SIMULATIONS

For the purpose of making empirical ROC curves, we first consider a noise corresponding to an autoregressive process : AR(6). The shape of its PSD is representative of a stellar PSD, with local variations (stellar oscillations) and higher energy at low frequencies (convection, magnetic activity). Under \mathcal{H}_1 , we consider the most general case $N_S > 1$. First of all, we evaluate the reliability of the $P_{\text{FA}}(\gamma)$, $P_{\text{DET}}(\gamma)$ and $P_{\text{DET}}(P_{\text{FA}})$ expressions for the \tilde{T} and \tilde{T}_{N_c} tests (Fig.1). We compare here our theoretical results (5), (17), (18), (19), (21) and (22) with 10^4 Monte Carlo (MC) simulations. The theoretical expressions are in agreement with the MC simulations and the test performances logically increase with L (as the estimation noise decreases).

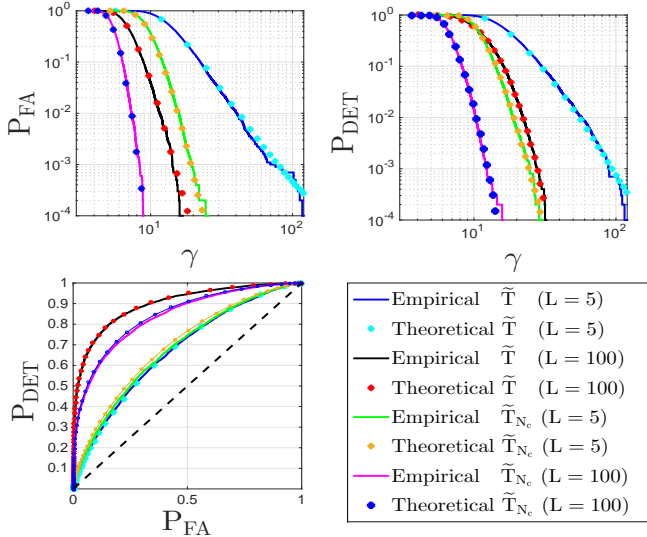


Fig. 1. Validation of the theoretical results for \tilde{T} and \tilde{T}_{N_c} by MC simulations. Parameters : $N = 1024$, $\Delta t = 60$ s, $N_s = N_c = 3$, $L = [5, 100]$, $\alpha_i = 0.1$ m/s for all sines, $f_i = [5, 5.75, 6.50]$ mHz.

In a second experiment, we place the different signal frequencies in a “valley” of the noise PSD (Fig.2.a). We calculate the empirical ROC curves (Fig.2.b) for the tests under study (see (10) to (14)). The figure shows that the performances of tests using \tilde{P} are better than those based on P in this configuration (violet, green and cyan curves on the diagonal). To gain more insight on the relative tests performances, we compare the frequency distribution under \mathcal{H}_0 of T_{Fi} and \tilde{T} (Fig.2.c, d). For T_{Fi} , the FA repartition is not uniform and increases in the PSD regions of larger energy ($\nu < 1$ mHz). When signals frequencies happen to fall into these zones, tests based on P are favored, but when they fall outside such regions their power vanish. In contrast, the \tilde{T} test allows a good detectability over all the frequency range, with performances close to the asymptotic one ($L \rightarrow \infty$, no estimation noise) for $L \approx 10^2$. In brief, the tests \tilde{T} and \tilde{T}_{N_c} allow to control precisely the P_{FA} , they have good power and their performances increase with L .

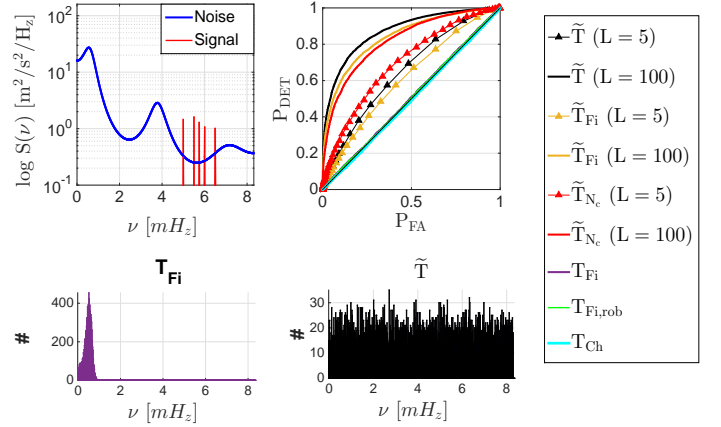


Fig. 2. (a) PSD of AR noise (blue) and sines (red). (b) ROC curves in case of signal frequencies falling into the PSD “valley” region : $N_c = N_s = 5$, $\alpha_i = 0.08$ m/s for all sines (the apparent amplitude difference is caused by the different leakage affecting these sines), $f_i = [5, 5.5, 5.75, 6, 6.5]$ mHz, with 10^4 simulations, $N = 1024$, $\Delta t = 60$ s, $L = [5, 100]$. (c, d) Histograms of the frequency distribution under \mathcal{H}_0 of $T_{Fi} = \max_n T_{Fi}(n)$ and $\tilde{T} = \max_n \tilde{T}(n)$.

Finally, we apply the tests (12) and (14) to real solar data [31] (Fig.3). These data have been collected for 18 years with an even sampling rate. As this data set is the largest one currently available we use it to compute ROC curves on shorter time series of $N = 1000$ samples extracted from the data set. In order to be as close as possible to the considered setting (perfect HD simulations of the stellar noise), we use part of the data to standardize the periodogram in (1). The left panel of Fig.3 superimposes the solar PSD (blue) with the introduced signals (red). The right panel displays the ROCs curves. The proposed standardized tests \tilde{T} , \tilde{T}_{Fi} and \tilde{T}_{N_c} (black, yellow and red) are more powerful than the others.

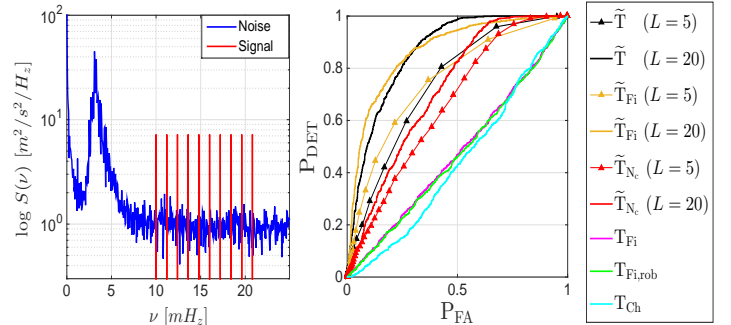


Fig. 3. Test on GOLF data. Parameters : $N = 10^3$, 4452 simulations for $L = 5$ and 1272 simulations for $L = 20$, $\Delta t = 20$ s, $N_s = N_c = 10$, $\alpha_i = 0.17$ m/s, $\{f_i\}$ equally spaced in $[10; 20]$ mHz.

8. CONCLUSION

We have investigated a detection method based on periodogram standardization through HD-simulation to counteract the impact of colored noise. We have analyzed its statistical performances and highlighted the shortcomings of tests ignoring the frequency dependence of the noise PSD. In contrast, the proposed standardization leads to a robust detection method in the sense that the P_{FA} is reliable and independent of the noise PSD. All theoretical results have been obtained in the asymptotic regime, but they appears to be a good approximation for relatively low values of N .

Acknowledgement We are grateful to Thales Alenia Space, PACA region and CNRS project DETECTION/Imag'In for supporting this work.

9. REFERENCES

- [1] G. R. Ricker et al., “Transiting Exoplanet Survey Satellite (TESS),” in *Society of Photo-Optical Instrumentation Engineers (SPIE)h Conference Series*, 2014, vol. 9143, p. 20.
- [2] H. Rauer and al., “The PLATO 2.0 mission,” *Experimental Astronomy*, vol. 38, pp. 249–330, 2014.
- [3] F. A. Pepe et al., “ESPRESSO : the Echelle spectrograph for rocky exoplanets and stable spectroscopic observations,” in *SPIE Conference Series*, 2010, vol. 7735.
- [4] D. A. Fischer et al., “Exoplanet Detection Techniques,” *Protostars and Planets VI*, pp. 715–737, 2014.
- [5] A. Schuster, “On the investigation of hidden periodicities,” *Journal of Geophysical Research*, vol. 3, pp. 13, 1898.
- [6] R. A. Fisher, “Tests of Significance in Harmonic Analysis,” *Royal Soc. of London Proc. Series A*, vol. 125, pp. 54–59, 1929.
- [7] S.T. Chiu, “Detecting periodic components in a white gaussian time series,” *J. R. Stat. Soc. Series B*, vol. 51, no. 2, pp. 249–259, 1989.
- [8] M. Shimshoni, “On fisher’s test of significance in harmonic analysis,” *Geophys J.R. Astronom*, pp. 373–377, 1971.
- [9] C. Zheng, “Detection of multiple sinusoids in unknown colored noise using truncated cepstrum thresholding and local signal-to-noise-ratio,” *Applied Acoustics*, pp. 809–816, 2012.
- [10] E. J. Hannan, “Testing for a jump in the spectral function,” *J. R. Stat. Soc. Series B*, vol. 23, no. 2, pp. 394–404, 1961.
- [11] M.B. Priestley, *Spectral Analysis and Time Series*, Academic Press, San Diego., 1981.
- [12] R. von Sachs, “Estimating the spectrum of a stochastic process in the presence of a contaminating signal,” *Signal Processing, IEEE Transactions on*, vol. 41, no. 1, pp. 323, Jan 1993.
- [13] R. von Sachs, “Peak-insensitive non-parametric spectrum estimation,” *Journal of Time Series Analysis*, vol. 15, no. 4, pp. 429–452, 1994.
- [14] S.T. Chiu, “Peak-insensitive parametric spectrum estimation,” *Stochastic Processes and their Applications*, vol. 35, pp. 121–140, 1990.
- [15] L.B. White, “Detection of sinusoids in unknown coloured noise using ratios of ar spectrum estimates,” *Proc. Information, Decision and Control*, pp. 257–262, 1999.
- [16] J.K. Gryca, “Detection of multiple sinusoids buried in noise via balanced model truncation,” *Instr. and Meas. Tech. Conf. IEEE*, vol. 2, pp. 1353–1358, 1998.
- [17] A. M. Zoubir, “Bootstrap : theory and applications,” in *SPIE Conference*, F. T. Luk, Ed., 1993, vol. 2027, pp. 216–235.
- [18] T.H. Li, *Time series with mixed spectra*, CRC Press, 2014.
- [19] J. A. Högbom, “Aperture Synthesis with a Non-Regular Distribution of Interferometer Baselines,” *ApJ*, vol. 15, pp. 417, 1974.
- [20] M. Tuomi et al., “Signals embedded in the radial velocity noise. Periodic variations in the τ Ceti velocities,” *A&A*, vol. 551, pp. A79, Mar. 2012.
- [21] X. Dumusque and al., “An Earth-mass planet orbiting α Centauri B,” *Nature*, vol. 491, pp. 207–211, 2012.
- [22] A. Hatzes, “The Radial Velocity Detection of Earth-mass Planets in the Presence of Activity Noise : The Case of α Centauri Bb,” *ApJ*, vol. 770, pp. 133, 2013.
- [23] L. Bigot et al., “The diameter of the CoRoT target HD 49933,” *A&A*, vol. 534, no. 3, 2011.
- [24] D.R. Brillinger, *Time Series : Data Analysis and Theory*, Holden Day, San Francisco, 1981.
- [25] M.S. Bartlett, “Periodogram analysis and continuous spectra,” *Biometrika*, vol. 37, pp. 1–16, 1950.
- [26] M. Abramowitz et al., *Spectral Analysis and Time Series*, Dover Publications, 1972.
- [27] N. Lu and D. Zimmerman, “Testing for directional symmetry in spatial dependence using the periodogram,” *Journal of Statistical Planning and Inference*, vol. 129, pp. 369–385, 2005.
- [28] A. Schwarzenberg-Czerny, “The distribution of empirical periodograms : Lomb–Scargle and PDM spectra,” *MNRAS*, vol. 301, pp. 831–840, 1998.
- [29] S.M. Kay, *Fundamentals of Statistical signal processing. Vol II : Detection theory.*, Prentice-Hall, Inc, 1998.
- [30] A. Siegel, “Testing for periodicity in a time series,” *Journal of the American Statistical Association*, vol. 75, no. 370, pp. 345–348, 1980.
- [31] R. A. Garcia et al., “Global solar Doppler velocity determination with the GOLF/SoHO instrument,” *A&A*, vol. 442, pp. 385–395, 2005.